ISME

Iranian Journal of Mechanical Engineering
The Iranian Society of Mechanical Engineers
Research Paper
DOI:10.30506/JMEE.2021.528341.1258

Numerical Investigation of the Circumferential Angle of the Axisymmetric Bypass Dual Throat Nozzle

M.H. Hamedi-Estakhrsar[*]
Ph.D

H. Mahdavy-Moghaddam[†]
Assistant Professor

One of the modern concept of Fluidic Thrust Vectoring (FTV) is the Bypass Dual Throat Nozzle (BDTN). In the present work this nozzle with a circular cross-section which is called ABDTN has been studied numerically. In this method a bypass channel separates the main nozzle flow into two parts as a primary and secondary flow from upstream of the nozzle throat. The results of the interaction between the main nozzle flow and the bypass channel flow are investigated as a secondary injection. The present work discusses about the performance parameters of the ABDTN, including thrust deflection angle, resultant thrust ratio, discharge coefficient, and thrust vectoring efficiency over a range of nozzle pressure ratios (NPR) to obtain the effects of different circumferential angles (α) of the bypass channel. The results of increasing α show that the maximum deflection angle will decrease from 24° to 21° at the nozzle pressure ratio of 1.5.

Keywords: Numerical Simulation, Axisymmetric Bypass Dual Throat Nozzle (ABDTN), Fluidic Thrust Vectoring (FTV), Thrust Ratio

1 Introduction

Mechanical and fluidic approaches are two common systems to implement thrust vector control. A mechanical TVC works by moving a nozzle or deflectors to change the direction of exhaust flow. Fluidic thrust vectoring in rocket technology generally precedes the current mechanical, electro-hydraulic gimbals. In the last two decades, in order to revamp an old technology into modern systems, the other concepts based on deflecting the nozzle exhaust flow without the use of mechanical actuators have emerged. Generally, fluidic thrust vectoring considers approaches as co-flow, counter-flow, shock vector control, throat skewing, and dual throat nozzle [1]. A system of FTV is lightweight, simple, without any movable parts, and inexpensive [2]. The new method of fluidic TVC is the dual throat nozzle (DTN) technique, which has higher thrust vectoring efficiency [3]. Flamm et al. [4] studied the geometric parameters of the DTN experimentally. Computational results of the axisymmetric DTN design show that the chocked secondary mass flow injection increases thrust deflection angle, but it has negative effects on the nozzle discharge coefficient up to 2% and resultant thrust ratio up to 1% [5].

[*] Ph.D., Department of Aerospace Engineering, K. N. Toosi University of Technology, Tehran, Iran, hadihamedi@email.kntu.ac.ir
[†] Assistant Professor, Department of Aerospace Engineering, K. N. Toosi University of Technology, Tehran, ran, mahdavy@kntu.ac.ir
Receive : 2021/04/15 Accepted : 2021/05/16

The dynamic response of the dual throat nozzle simulated in open loop and close loop control by Ferlauto and Marsilio [6]. Hamedi-Estakhrsar et al. [7] analyzed different convergent and divergent angles for different working conditions of the nozzle. Numerical investigation is performed on the planar nozzle with different divergence angles [8]. Fluidic thrust vectoring performance parameter is computed by experimental tests and numerical simulations using thrust pitching moment and thrust pitching angle [9]. Secondary flow injection in a supersonic square duct is investigated numerically by Yang et al. [10]. The newest type of fluidic thrust vector control method, entitled bypass dual throat nozzle (BDTN), is proposed to decrease thrust loss due to the bleeding air. In other words, this method can generate only thrust vector by nozzle itself, without the requirement of extract the bypass mass flow from the other part of an engine. Gu et al. [11, 12] proposed a model of BDTN that can generate efficient and steady thrust deflection without any injecting secondary mass flow experimentally and numerically. The dynamic response of the BDTN has been studied experimentally [13]. The results represent that in addition to the efficient deflection, the BDTN can respond very quickly. Wang et al. [14] investigated the effects of the bypass width on the performance of axisymmetric BDTN at the fixed geometry. Also, the 3-D effects on the flow structure inside the nozzle have been studied [15]. Recently, Hamedi-Estakhrsar et al. [16, 17] investigated the controllability of the BDTN and the performance evaluation at different operation conditions numerically and experimentally. According to above literature review, it can be concluded that there is not any investigation about the axisymmetric bypass dual throat nozzle (ABDTN) with circular cross section to show the effects of circumferential angles of bypass channels on the thrust vectoring overall performance of this concept and its losses.

Therefore in the present work, an axisymmetric model of the BDTN is introduced and also in addition to common fluidic thrust vectoring performance parameter including thrust deflection angle (δ), resultant thrust ratio (C_f), and discharge coefficient (C_d) the relationships between the nozzle pressure ratio and some parameters such as thrust vectoring efficiency, axial and normal forces, secondary mass flow rate, thrust amplification factor and skin friction coefficient are investigated numerically. Finally, the obtained results of various circumferential angles of bypass channels are presented.

2 ABDTN Geometry Configuration

The geometry configuration of the axisymmetric bypass dual throat nozzle is presented in Figure (1). The baseline geometry of the BDTN has been studied by Gu et al. [11]. The results of the static pressure distribution on the nozzle sidewalls are available for this nozzle configuration with rectangular cross section experimentally and numerically [11]. The scaled down (1:2) geometrical dimensions of the BDTN are given in Table (1) in details.

3 Numerical Approach

The commercial Ansys Fluent 17 is used for carrying out the numerical simulations. The fluid flow is governed by the 3-D, steady-state and compressible Reynolds Averaged Navier-Stokes (RANS) equations. The density-based solver is selected for the numerical simulations of the supersonic airflow through the ABDTN. The scheme of Second-Order Upwind is utilized for spatial discretization.

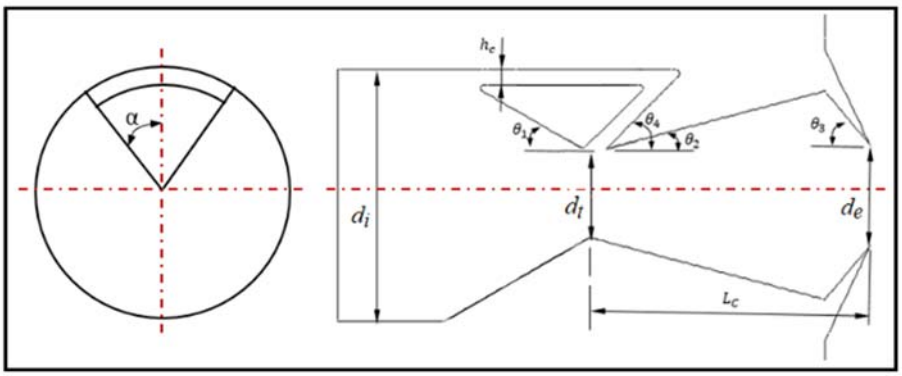

Figure 1 Geometry description of the ABDTN

Table 1 Details of ABDTN configuration

Parameter	Definition	Value
d_t	Throat Diameter	10 mm
d_i/d_t	Inlet Diameter	3
d_e/d_t	Outlet Diameter	1.2
h_c/d_t	Height of Bypass Channel	0.185
L_c/d_t	Length of Cavity	3.34
α	Circumferential Angle	30º, 45º
θ_1	Nozzle Convergence Angle	30º
θ_2	Cavity Divergence Angle	15º
θ_3	Cavity Convergence Angle	50º
θ_4	Bypass Channel Angle	45º

The boundary conditions adopted at each edge of the computational domain are resumed in Figure (2). For the entrance of nozzle the Pressure Inlet boundary condition is considered. The primary airflow inside of the nozzle at the inlet is set to a fixed total temperature of 300 *K* and total pressure of 1013025 *Pa*. Turbulence modeling of inlet boundary condition is set to the nozzle hydraulic diameter and turbulence intensity of 3%. The Pressure Outlet, is set to the downstream boundary condition with a different specified static pressure to achieve the particular NPR. The discharge ambient boundaries have been computed by using the Pressure Far-field condition with a very small Mach number of M=0.01 (See Figure (2)).
In the numerical study, the half of the nozzle geometry is computed by introducing a plane of symmetry to decrease the time and cost of simulations. This plane contains the axis of symmetry of the nozzle and splits the bypass channel in half. The No-Slip boundary condition at the solid walls of the nozzle is imposed on the airflow velocity components.

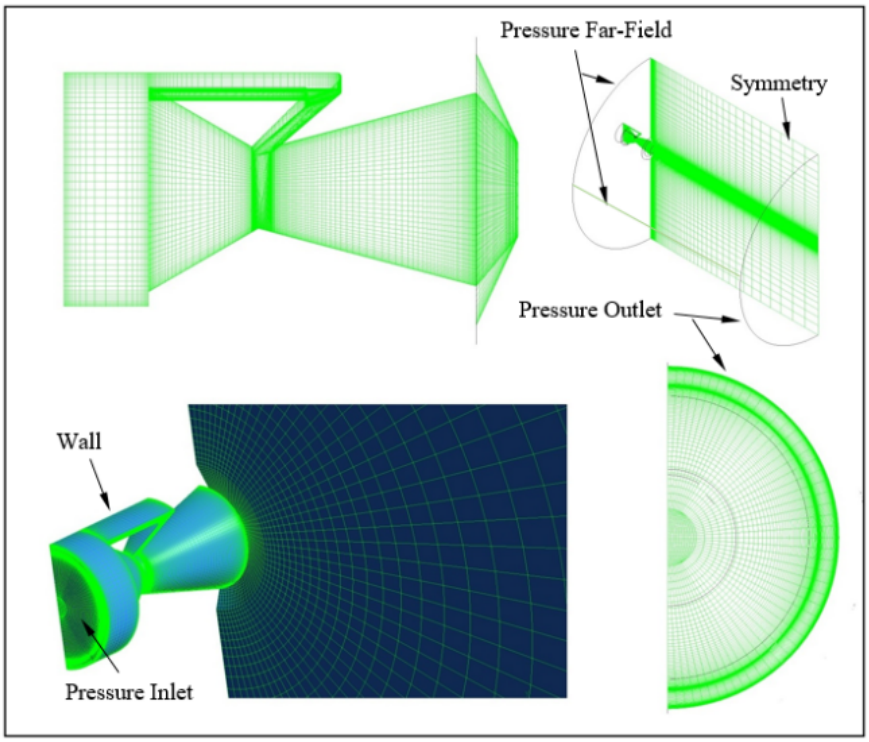

Figure 2 Computational grid and boundary conditions

The grid independency of numerical solution has been performed by comparing the obtained results of different grids. A coarse mesh (Grid A), a medium-mesh (Grid B), and a finer mesh (Grid C) have been used with a total number of nodes of about 0.2, 0.6, and 0.9 million nodes, respectively. Figure (3a) represents the obtained results of the pressure distribution on the nozzle up-wall using the above-mentioned grids at NPR=3. It seems that the Grid B obtains the grid-independent solution. For this grid, the maximum value of $y^+ \simeq 1$ along the nozzle is considered to meet the criteria of the SST k-ω turbulence model. Moreover at least 10 cells have been created near wall region to be able to resolve the turbulent quantities and mean velocity in the viscosity affected region.
Figure (2) shows the 3-D Medium mesh of the computational domain and near the ABDTN. In order to obtain an independent computational domain, the nozzle outlet region has been extended along the x-direction and the y-direction by 30 and 12 times of outlet diameter of nozzle, respectively.

4 Turbulence Modelling

Gu et al. [11-13] have used the RNG k-ε turbulence model with standard wall function for the flow inside the geometry of bypass dual throat nozzle with a rectangular cross-section. Wang et al. [15] have compared the ability of the three turbulence models. The turbulence models, including the realizable k-ε (RKE), Spalart-Allmaras (SA), and SST k-ω are used in their investigations. They concluded that the SA and SST k-ω are appropriate for simulation of the airflow field and for capturing the complex shock waves inside and outside of the dual throat nozzle. In conclusion, in the present work, the SST k–ω turbulence model [18] is considered to solve the airflow filed into the ABDTN and to calculate the performance parameters of thrust vectoring.

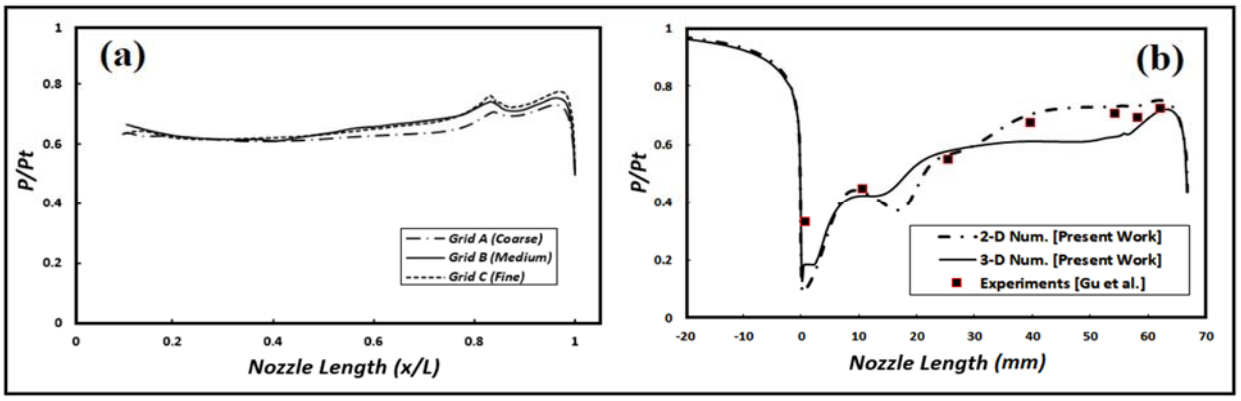

Figure 3 Pressure distribution at NPR=3 (a) grid study on the nozzle up-wall and (b) validation of results on the nozzle down-wall

The governing equations of mass, momentum, and energy balance, are as follows

$$\frac{\partial \rho}{\partial t}+\frac{\partial}{\partial x_i}\left(\rho u_i\right)=0 \tag{1}$$

$$\frac{\partial}{\partial t}\left(\rho u_i\right)+\frac{\partial}{\partial x_j}\left(\rho u_i u_j\right)=-\frac{\partial p}{\partial x_i}+\frac{\partial}{\partial x_j}\left[\mu\left(\frac{\partial u_i}{\partial x_j}+\frac{\partial u_j}{\partial x_i}-\frac{2}{3}\delta_{ij}\frac{\partial u_k}{\partial x_k}\right)\right]+\frac{\partial}{\partial x_j}\left(-\rho\overline{u_i' u_j'}\right) \tag{2}$$

$$\frac{\partial}{\partial t}\left(\rho E\right)+\frac{\partial}{\partial x_i}\left[u_i\left(\rho E+p\right)\right]=\frac{\partial}{\partial x_j}\left[\left(k+\frac{C_p\mu_t}{P_{rt}}\right)+u_i\left(-\rho\overline{u_i' u_j'}\right)\right] \tag{3}$$

The terms of u is mean quantity of velocity, whereas u_0 is a fluctuating quantity. The terms of $(-\rho\overline{\acute{u}_i\acute{u}_j})$ represent the Reynolds stress tensor.

5 Results and Discussion

The common performance parameters of thrust vector control approaches are resultant thrust ratio C_f, thrust deflection angle δ, discharge coefficient C_d and thrust vectoring efficiency η [1]. The present investigation measures the performance parameters of the axisymmetric bypass dual throat nozzle (ABDTN). The system resultant thrust ratio (C_f) is calculated by the ratio of the resultant measured thrust of nozzle to the ideal thrust [19].

$$C_f=\frac{\sqrt{{F_A}^2+{F_N}^2}}{F_i} \tag{4}$$

Where F_A and F_N are the measured value of axial and normal force component, respectively. The isentropic thrust of the ABDTN is defined by F_i. The thrust deflection angle is defined for evaluating the performance of the FTV system as following

$$\delta=tan^{-1}\frac{F_N}{F_A} \tag{5}$$

The nozzle discharge coefficient C_d is determined by

$$C_d=\frac{\dot{m}_a}{\dot{m}_i} \tag{6}$$

In this formula C_d is the ratio of the actual mass flow to the ideal one. As described here, $\dot{m}_a$ and $\dot{m}_i$represent the actual and ideal mass flow rate of ABDTN, respectively.
The thrust-vectoring efficiency is determined by

$$\eta = \frac{\delta}{(\frac{w_s}{w_p + w_s}) \times 100} \tag{7}$$

Where δ represent the thrust deflection angle (measured in degrees) and w_p is the primary nozzle mass flow rate. Skin friction coefficient (C_w) is a non-dimensional parameter defined by

$$C_w = \frac{\tau_w}{\frac{1}{2}\rho v^2} \tag{8}$$

Where τ_w is the wall shear stress, and ρ and v are the nozzle inlet density and velocity, respectively. Basically, the flow field through the ABDTN is similar to that of the pure DTN [4, 5]. The previous investigations have presented that the internal flow of dual throat nozzle is dominated by two standing vortices trapped in the diverging-converging region between two throats. Deree et al. [5] used a specific configuration of DTN to determine the effect of slot circumferential injection on thrust vectoring and internal nozzle performance. They investigated this parameter only at the NPR of 1.89 with a nominal 3% injection of secondary mass flow. While in the present work, the ABDTN performance is evaluated at the range of nozzle pressure ratio of 1.5-4.5 and at different secondary mass flow rates of bypass duct.
The main goal of this section is to investigate the influence of the circumferential angle of bypass channel (α) on the performance of ABDTN at different NPRs. The predicted results present that the selected solver able to predict the trend of thrust vectoring performance parameters for axisymmetric bypass dual throat nozzle. Thus all simulations have been carried out by using above mentioned numerical solver. The numerically obtained results of the effects of α on the angle of thrust vector deflection are presented in Figure (4a). The predicted results show that the ABDTN geometry with α=30º can deflect the airflow about 16º at nozzle pressure ratio of 4.5. When the nozzle pressure ratio increases, δ will reduce. Also, by increasing the circumferential angle from 30º to 45º, the maximum deflection angle will decrease from 24º to 21º at the nozzle pressure ratio of 1.5 (with 13% reduction). The effect of circumferential angle on the thrust ratio in terms of NPR is illustrated in Figure (4b). As shown in this figure by increasing α=30º to 45º, the C_f will decrease about 1.5%. When the nozzle pressure ratio increases from 1.5 to 4.5, the C_f will increase from 0.8 to 0.95 for the configuration of α=30º. The discharge coefficient of the ABDTN is determined with different α at the different nozzle pressure ratios (see Figure (4c)). This figure shows that the quantities of C_d is approximately independent of the circumferential angle of the bypass channel because the difference between these configurations is smaller than 1 %, although it will decrease when α increases. The studied different configurations of axisymmetric dual throat nozzle able to change discharge coefficient in the range of 0.8 to 0.85 at the NPR of 2-4.5. In general, the thrust vectoring efficiency applies to the applications in which the second mass flow injects from another part of an engine or the other source. In the present study, the fluid flow in the ABDTN is investigated without any secondary injection from out of the nozzle. Therefore, despite the fact that thrust vectoring efficiency is not common for this geometry but this parameter is used to the comparison of thrust vectoring performance of different configurations.
Figure (4d) shows the effect of different configurations of ABDTN on η at various nozzle pressure ratios. By increasing the nozzle pressure ratio the thrust vectoring efficiency will generally reduce. Moreover, for configuration with α=30º, the thrust vectoring efficiency is 3.2 at nozzle pressure ratio of 1.5 and then decrease to η=2 at NPR =4.5. The axisymmetric bypass dual throat nozzle configuration with α=30º generates substantially larger thrust vectoring efficiency than geometry with α=45º over the entire range of NPR.

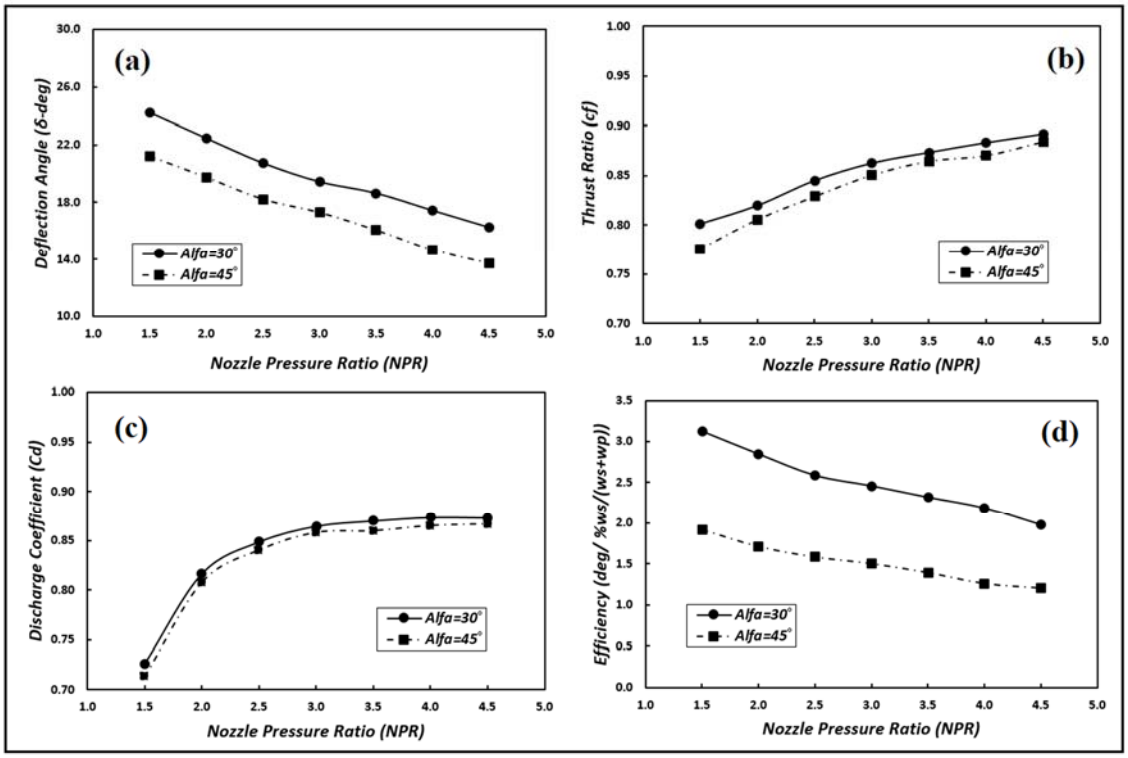

Figure 4 Effects of α on (a) thrust deflection angle, (b) thrust ratio, (c) discharge coefficient, and (d) thrust vectoring efficiency

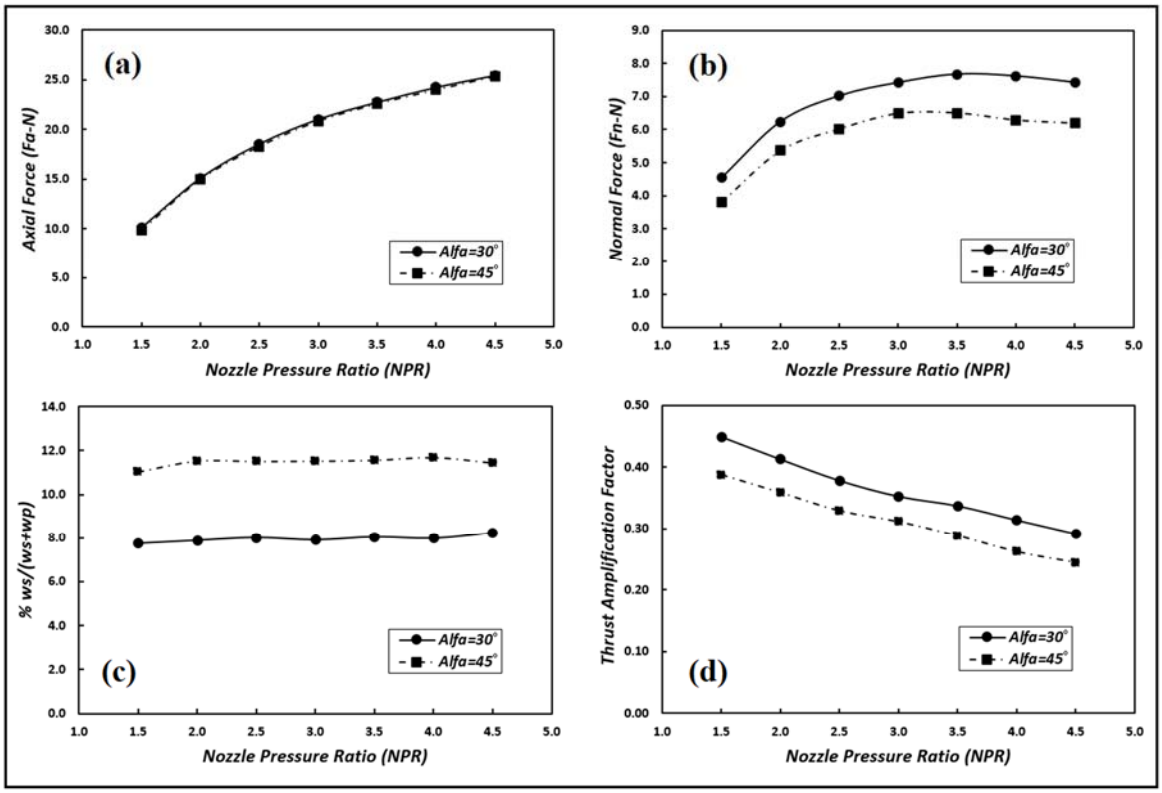

Figure 5 Effects of α on (a) axial force, (b) normal force, (c) secondary mass flow, and (d) thrust amplification factor

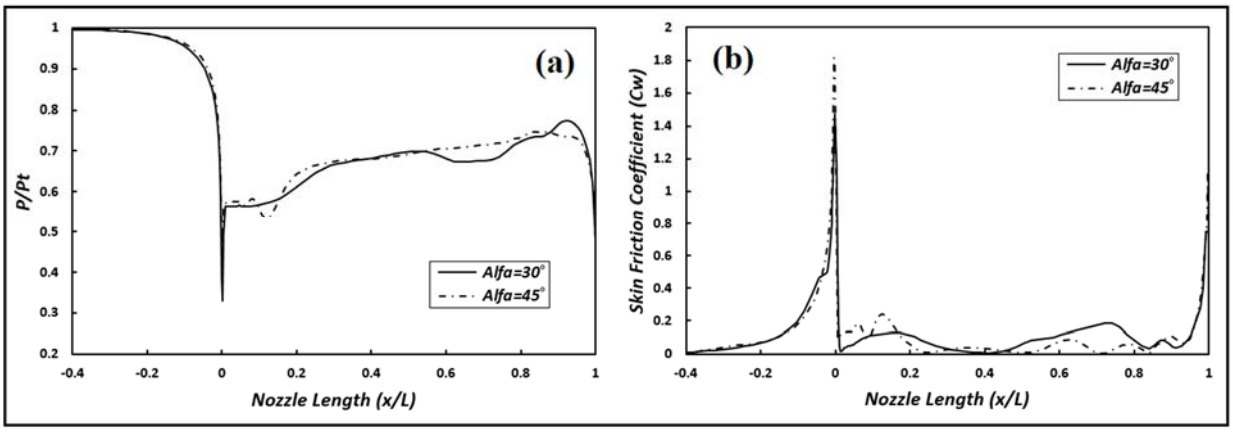

Figure 6 Predicted results on nozzle down-wall at NPR=3 (a) pressure distribution and (b) skin friction coefficient (C_w)

In addition to the common performance parameters of fluidic thrust vectoring systems the diagrams of the axial F_a and normal F_n nozzle force components are presented in Figures (5a) and (5b), respectively. It seems that the higher thrust deflection angles are actually due to a relative increase of F_n toward the constant behavior of the axial thrust component F_a.

The secondary mass flow rate in terms of nozzle pressure ratio is presented in Figure (5c) for different configurations of ABDTN. This figure shows that the percentage of secondary mass flow injection rates ($\%w_s/(w_s+w_p)$) changes almost linear with NPR for different configurations of the nozzle. Moreover, by changing α from 30º to 45º, the bypass flow will increase from 8% to 11.5%. As a result, the increase of the secondary mass flow leads to loss of thrust ratio and normal force. `The thrust amplification factor is defined in terms of a ratio of side force to axial force specific impulse. In the present study, the results of this parameter as a thrust vectoring effectiveness are shown Figure (5d). It seems that by changing the circumferential angle of the bypass channel from 30º to 45º, the thrust amplification factor will decrease about 15%.

Pressure distribution and skin friction coefficient on the intersection of nozzle down-wall and symmetry plan at the NPR=3 for different configurations of ABDTN are plotted in Figure (6). For a more detailed discussion, the variation of pressure on the nozzle down-wall is illustrated in Figure (6a). As shown, by increasing α, the position of the normal shock moves from the first throat to the nozzle outlet.

The predicted results indicate that the flow inside the nozzle did not reattach to the nozzle wall a little bit after the first throat for configuration with α=30 and so it causes separation. While this phenomenon will happen after the 20% of nozzle length for α=45 . On the other hand, by decreasing the circumferential angle of the bypass channel, the separation point occurs near the nozzle throat (see Figure (6b)).

Finally, Figure (7) shows the streamline of airflow of different configurations of the bypass channel at the fixed NPR=3. This figure shows that when α increases from 30º to 45º, the value of thrust deflection angle will decrease. When the second mass flow rate increases due to the increasing circumferential angle of the bypass channel, the secondary flow applies more force to the primary flow. It leads to trapping flow at the end of the diverging zone of the down-wall. As a consequence, increasing the circumferential angle of the bypass duct has an adverse effect on the performance parameters of the ABDTN.

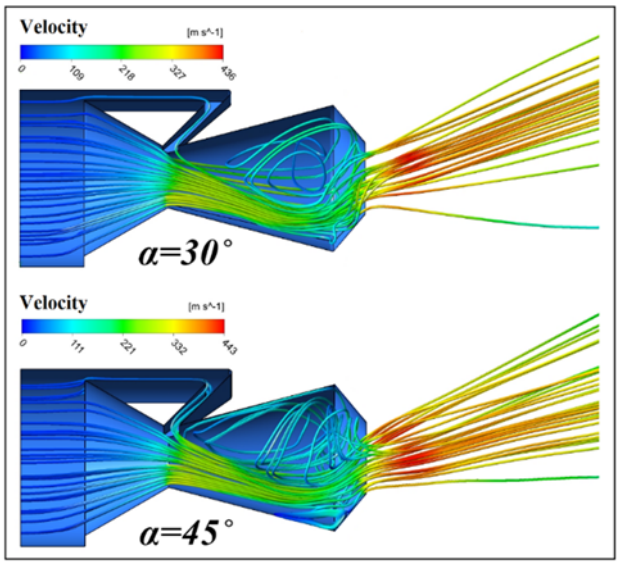

Figure 7 Effects of α and streamline of airflow at the NPR=3

As a result, the 30º circumferential secondary channel had the best discharge coefficient and thrust ratio because the smaller α leads to the least amount of flow separation in the cavity. Therefore, this configuration is chosen to apply thrust vectoring experiments and simulations of this work.

6 Conclusion

In the present study, the effect of circumferential angle of the axisymmetric bypass dual throat nozzle (ABDTN) on the resultant thrust ratio (C_f), discharge coefficient (C_d), and thrust deflection angle (δ) have been investigated for various nozzle pressure ratios numerically. Some of most important results are:

- The agreement of the predicted results with experimental data shows the ability of the selected numerical simulation approach to evaluate the performance of 3-D turbulent airflow inside the ABDTN.
- The configuration of ABDTN with the circumferential angle of bypass channel of 30º is provided the best thrust vectoring efficiency and nozzle performance over the range of nozzle pressure ratio.
- Increasing the value of α has an adverse effect on the thrust amplification factor of ABDTN method.
- The results of C_d is approximately independent of the circumferential angle of bypass channel.

References

[1] Kexin, W., Heuy, D. K., and Yingzi, J., "Fluidic Thrust Vector Control Based on Counter-Flow Concept", Proc IMechE Part G: J Aerospace Engineering. Vol. 233, No. 4, pp. 1412-1422, (2019).

[2] Mason, M.S., and Crowther, W.J., " Fluidic Thrust Vectoring of Law Observable Aircraft", In: CEAS Aerospace Aerodynamic Research Conference, Cambridge, UK, (2002).

[3] Deere, K.A., Berrier, B.L., Flamm, J.D., and Johnson, S.K., " A Computational Study of a New Dual Throat Fluidic Thrust Vectoring Nozzle Concept", AIAA Paper, No. 2005-3502, (2005).

[4] Flamm, J.D., Deere, K.A., Mason, M., Berrier, B.L., and Johnson, S.K., "Design Enhancements of the Two Dimensional, Dual Throat Fluidic Thrust Vectoring Nozzle Concept", In: 3rd AIAA Flow Control Conference, San Francisco, CA, United States, AIAA Paper, No. 2006-3701, (2006).

[5] Deere, K.A., Flamm, J.D., Berrier, B.L., and Johnson, S.K., "Computational Study of an Axisymmetric Dual Throat Fluidic Thrust Vectoring Nozzle Concept for Supersonic Aircraft Application", AIAA, Paper No. 2007-5085, (2007).

[6] Ferlauto, M., and Marsilio, R., "Numerical Investigation of the Dynamic Characteristics of a Dual-throat Nozzle for Fluidic Thrust-Vectoring", AIAA Journal, Vol. 55, pp. 86-98, (2017).

[7] Hamedi Estakhrsar, M.H., Mahdavy Moghaddam, H., and Jahromi, M., "Investigation of Effects of Convergence and Divergence Half-angles on the Performance of a Nozzle for Different Operating Conditions", J. Braz. Soc. Mech. Sci. Eng. Vol. 40, pp. 353-362, (2018).

[8] Nair, P.P., Suryan, A., and Kim, H.D., "Computational Study on Reducing Flow Asymmetry in Over-expanded Planar Nozzle by Incorporating Double Divergence", Aerosp. Sci. Technol., (2020), DOI: 10.1016/j.ast.2020.105790.

[9] Li, L., Hirota, M., Ouchi, K., and Saito, T., "Evaluation of Fluidic Thrust Vectoring Nozzle via Thrust Pitching Angle and Trust Pitching Moment", Shock Waves, Vol. 27, pp. 53-61, (2017).

[10] Yang, R., Wang, Z.G., Zhao, Y.X., Wang, Q.C., and Feng, W.H., "Numerical Investigation on Spatial Development of the Secondary Flow in a Supersonic Turbulent Square Duct", Aerosp. Sci. Technol., (2020), DOI: /10.1016/j.ast.2020.105832.

[11] Gu, R., Xu, J.L., and Guo, S., "Experimental and Numerical Investigations of a Bypass Dual Throat Nozzle", J. Eng. Gas Turbines Power, Vol. 136, 084501, (2014).

[12] Gu, R., and Xu, J.L., "Effects of Cavity on the Performance of Dual Throat Nozzle During the Thrust-vectoring Starting Transient Process", J. Eng. Gas Turbines Power, Vol. 136, 014502, (2014).

[13] Gu, R., and Xu, J.L., "Dynamic Experimental Investigations of a Bypass Dual Throat Nozzle", J. Eng. Gas Turbines Power, Vol. 137, 084501, (2015).

[14] Wang, Y., Xu, J., Huang, S., Lin, Y., and Jiang, J., "Computational Study of Axisymmetric Divergent Bypass Dual Throat Nozzle", Aerosp. Sci. Technol. Vol. 86, pp. 177-190, (2019).

[15] Wang, Y., Xu, J., Huang, S., Lin, Y., and Jiang, J., "Experimental and Numerical Investigation of an Axisymmetric Divergent Dual Throat Nozzle", Proc IMechE Part G: J Aerospace Engineering, Vol. 0, pp. 1-10, (2019).

[16] Hamedi Estakhrsar, M.H., Ferlauto, M., and Mahdavy Moghaddam, H., "Numerical Study of Secondary Mass Flow Modulation in a Bypass Dual-throat Nozzle", Proc IMechE Part G: J Aerospace Engineering, (2020). DOI: 10.1177/0954410020947920.

[17] Hamedi Estakhrsar, M.H., and Mahdavy Moghaddam, H., "Experimental Evaluation and Numerical Simulation of Performance of the Bypass Dual Throat Nozzle", Proc IMechE Part G: J Aerospace Engineering, (2020). DOI: 10.1177/0954410020959886.

[18] Menter, F.R., "Two-equation Eddy-viscosity Turbulence Models for Engineering Applications", AIAA J., Vol. 32, pp. 1598-1605, (1994).

[19] Deere, K.A., Berrier, B.L., Flamm, J.D., and Johnson, S.K., "Computational Study of Fluidic Thrust Vectoring using Separation Control in a Nozzle", AIAA, Paper No. 2003-3803, (2003).

Nomenclature

Notations

A_t	Nozzle Throat Area (m^2)
C_d	Discharge Coefficient
C_f	Resultant Thrust Ratio
d_t	Throat Diameter (m)
F_n	Normal Force (N)
F_a	Axial Force (N)
F_i	Ideal Isentropic Force(N)
k	Turbulent Kinetic Energy (m^2/s^2)
L_c	Length of Cavity (mm)
$\dot{m}_a$	Actual (Measured) Mass Flow Rate (kg/s)
$\dot{m}_i$	Ideal Mass Flow Rate (kg/s)
N	Number of Samples
P_0	Total Pressure (Pa)
R	Gas Constant ($kj/kg\ K$)
T_0	Total Temperature (K)
V	Airflow Velocity (m/s)

w_p	Primary Mass Flow Rate (*kg/s*)
w_s	Secondary Mass Flow Rate (*kg/s*)

Greek Symbols

α	Circumferential Angle of Bypass Channel (º)
γ	Specific Heat Ratio
Γ_k	Effective Diffusivity of k
Γ_{ω}	Effective Diffusivity of ω
δ	Thrust Deflection Angle (º)
η	Thrust Vectoring Efficiency
θ	Cavity Angle (º)
μ_t	Turbulent Dynamic Viscosity (*Pa.s*)
σ_k	Turbulent Prandtl Numbers for k
σ_{ω}	Turbulent Prandtl Numbers for ω
σ	Variance of Measured Data

Abbreviations

ABDTN	Axisymmetric Bypass Dual Throat Nozzle
BDTN	Bypass Dual Throat Nozzle
DTN	Dual Throat Nozzle
FTV	Fluidic Thrust Vectoring
NPR	Nozzle Pressure Ratio
TVC	Thrust Vector Control